WARSAW UNIVERSITY OF TECHNOLOGY Index 351733
FACULTY OF CIVIL ENGINEERING
COMMITTEE FOR CIVIL AND WATER ENGINEERING
POLISH ACADEMY OF SCIENCES ISSN 1230-2945

DOI: 10.24425/ace.2020.131805
ARCHIVES OF CIVIL ENGINEERING
Vol. LXVI ISSUE 2 2020

NUMERICAL ANALYSIS OF ROAD ACOUSTIC SCREEN

P. STEMPIN[1], W. SUMELKA[2]

This article presents the results of a numerical analysis of the road acoustic screen deterioration. Due to the fact that road noise barriers are located in an environment of very high corrosivity, the problem is the rusting of the metal cladding of component panels. The presented case study was, therefore, verified to fulfill the requirements presented in the Eurocode EN 1794-1. Static analysis for wind load and dynamic analysis for the load induced from vehicles was carried out. The analysis presented in the article proved the design errors and their contribution to the formation of severe corrosion, as well as demonstrating the importance of dynamic analysis in the design of acoustic screens.

Keywords: acoustic screen, corrosion, numerical analysis

1. INTRODUCTION

The purpose of the acoustic screen is to reduce the noise generated by car traffic. Different construction materials can be used for screen, e.g.: wool in a metal casing, glass, precast concrete, ceramic or wood [1,2]. To reduce noise, also earth embankments, slopes, and green belt lands can be used, but the most common are vertical barriers in the form of acoustic screens. The applied solutions are mainly based on acoustic performance [3,4] and aesthetic factors [5,6], but strength and durability [7] must be taken into account also.

Acoustic screens consist of structural elements and acoustic elements. Structural elements are most commonly steel columns fixed in foundation piles. Their static scheme is a cantilever. The

[1] M.Sc., Eng., Poznan University of Technology, Institute of Structural Analysis, Piotrowo 5, 60-965 Poznan, Poland, e-mail: paulina.s.stempin@doctorate.put.poznan.pl

[2] DSc., PhD., Eng., Prof. PUT, Poznan University of Technology, Institute of Structural Analysis, Piotrowo 5, 60-965 Poznan, Poland, e-mail: wojciech.sumelka@put.poznan.pl

columns are a support structure for acoustic panels and a ground beam. In addition, the ground beam is simple-supported on the heads of piles and provides support for acoustic panels.

Construction elements of acoustic screens should be designed for 30 years of life and acoustic elements for 15 years [8], therefore must be resistant to loads from death weight, wind pressure, aerodynamic load caused by car traffic, impacts of snow discarded during snow removal or stone hittings [9,10]. Significantly important is the fluctuating pressure caused by passing vehicles [11], [12] by reason of the dynamic response of acoustic screen [13]. Furthermore, the resistance to environmental condition should be considered also [7].

Due to the proximity of the road lane, noise barriers work in an environment with high or very high corrosivity (category C4 or C5 [14]). It may cause corrosion [15,8]: moisture (dew, precipitation, contact with snow and ice), chlorides from road de-icing substances, sulfur, nitrogen and carbon compounds from car exhaust fumes, impurities such as sand and dust. In addition, mechanical damage caused by the impact of stones discarded from the wheels of cars and the formation of gaps and scratches may initiate the beginning of corrosion. Therefore, especially screens made of steel or aluminum are exposed to corrosion.

Aluminum, so also aluminum cladding, is primarily exposed to electrochemical (galvanic), pitting or crevice corrosion [16]. In particular, in the conditions of strong acidity or alkalinity, the rate of corrosion is high and has usually localized nature [17]. Galvanic corrosion [18] occurs in a conductive environment (road splash containing deicing salts) when aluminum is in contact with dissimilar metal. Pitting corrosion of aluminum [19,20,21] is caused primarily by chlorides. Crevice corrosion [22,23] is similar to the pitting, with the difference that for crevice corrosion a gap is necessary [16,24].

This article presents the results of a numerical analysis of the acoustic screen deterioration located on the expressway S11 in Skrzynki (Kórnik, Poland) next to Kórnik-North junction, in which damage associated with corrosion of the material was observed (Fig. 1). The analysis was aimed at finding the causes of such severe corrosion. Static and dynamic effects of loads were taken into account and the correctness of acoustic screen design was checked in accordance with the applicable standards. It should be additionally emphasized that the meaningful role of dynamics in acoustic screen design was demonstrated.

2. GEOMETRY OF ACOUSTIC SCREEN

In the presented case study the acoustic screen consists of acoustic panels, a ground beam, and a support structure, which are steel columns fixed in concrete piles (see Fig. 2, 3). The panels

are composed of the following elements [1]:

- external cladding made of profiled aluminum sheet, 1 mm thick, full – without perforation,
- the adhesive layer, 0,5 mm thick,
- core made of mineral wool, 123 mm thick,
- the adhesive layer, 0,5 mm thick,
- external cladding made of profiled aluminum sheet, 1 mm thick, perforated,
- side aluminum frames made of C-section 125x125x0,5 mm,
- four rubber gaskets.

Fig. 1. Corroded acoustic screens on the expressway S11 in Skrzynki (Poland) next to Kórnik-North junction

The acoustic elements are connected with each other by the tongue and groove method. The analyzed screen consists of 10 panels. The geometry of the road noise barrier and the cross-section are presented in Fig. 2 and Fig. 3, respectively. Fig. 4 presents a cross-section through a single panel.

3. MECHANICAL REQUIREMENTS ACCORDING TO EN 1794-1

In addition to acoustic conditions, the Eurocodes [9,10] specify the requirements for an acoustic screen as an independent construction. Eurocode [9] primarily defines the maximum permissible horizontal displacements for individual screen elements. The particular conditions are summarized in Table 1. Furthermore, the Eurocode [9] indicates that the dead weight of the acoustic elements should be taken in a wet state, i.e. having pores of the material filled with water.

Moreover, it is necessary to prevent separation between individual panels, non-reversible displacement of acoustic elements and detachment from supports or fixings and the creation of permanent deformation [9]. For the analyzed acoustic screen, the permissible elastic

deflection for wind load or load caused by car traffic is 36,7 mm for structural element and 50 mm for an acoustic element

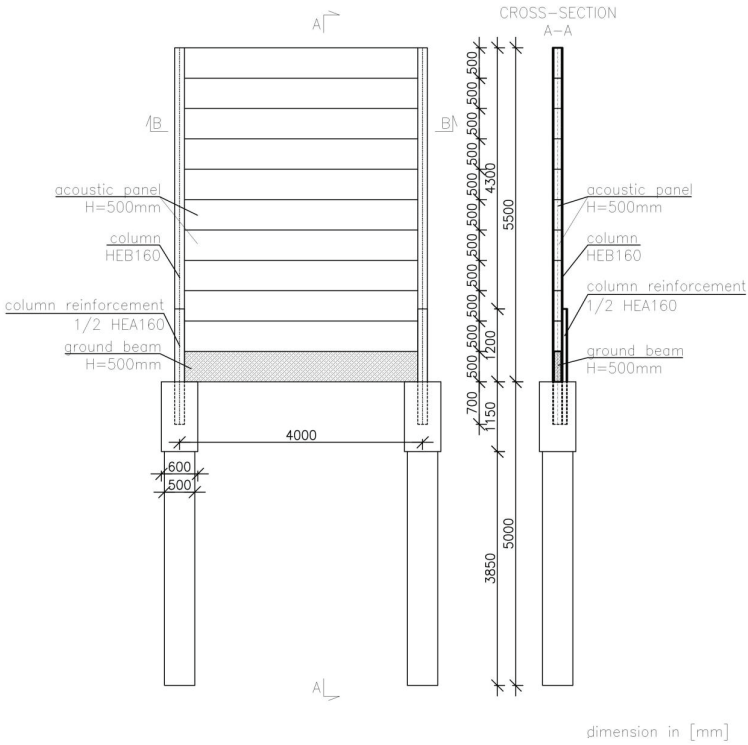

Fig. 2. The geometry of a single acoustic screen

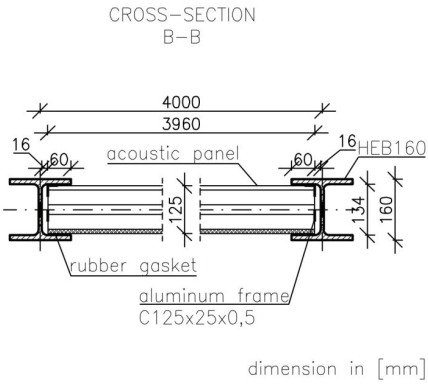

Fig. 3. Cross-section of the acoustic screen (cf. Fig. 2)

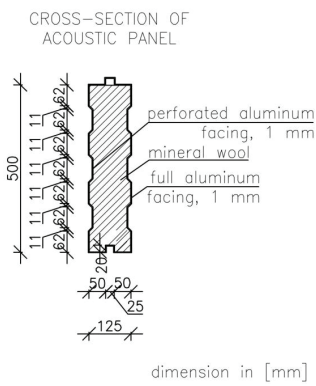

Fig. 4. Cross-section of the acoustic panel

Table 1. Permissible deflection

Type of load	Elastic deflection		Non-reversible deflection	
	Structural element	Acoustic element	Structural element	Acoustic element
Wind	$d_{h_{max}} = \frac{L_S}{150}$	50 mm	$d_{h_{max}} = \frac{L_S}{500}$	$d_{h_{max}} = \begin{cases} \frac{L_A}{500} \\ \frac{h}{500} \end{cases}$
Load caused by car traffic	$d_{h_{max}} = \frac{L_S}{150}$	50 mm	$d_{h_{max}} = \frac{L_S}{500}$	$d_{h_{max}} = \begin{cases} \frac{L_A}{500} \\ \frac{h}{500} \end{cases}$
Dead weight	not specified	not specified	not specified	$d_{h_{max}} = \frac{h}{50}$
Snow	not specified	not specified	not specified	not specified
where: L_S – the largest length of the structural element, in mm, L_A – the largest length of the acoustic element, in mm, h – total height of the acoustic element, in mm,				

4. NUMERICAL MODEL OF THE ACOUSTIC SCREEN

The 3-D model for a single noise barrier was prepared in the ABAQUS system. The following material and cohesive models were used in the computations:

- Elastic, isotropic for aluminum, steel, and concrete (Table 2), where the stress is defined as a linear function of elastic strain [25]

$$\boldsymbol{\sigma} = \boldsymbol{D}\boldsymbol{\varepsilon} = \frac{E}{(1+\nu)(1-2\nu)} \begin{bmatrix} 1-\nu & \nu & \nu & 0 & 0 & 0 \\ \nu & 1-\nu & \nu & 0 & 0 & 0 \\ \nu & \nu & 1-\nu & 0 & 0 & 0 \\ 0 & 0 & 0 & \frac{1-2\nu}{2} & 0 & 0 \\ 0 & 0 & 0 & 0 & \frac{1-2\nu}{2} & 0 \\ 0 & 0 & 0 & 0 & 0 & \frac{1-2\nu}{2} \end{bmatrix} \boldsymbol{\varepsilon}\,, \tag{4.1}$$

where: $\boldsymbol{\sigma}$ – stress matrix, $\boldsymbol{D}$ – constitutive matrix, $\boldsymbol{\varepsilon}$ – strain matrix, E – Young's modulus, ν – Poisson's ratio.

- Hyperelastic, isotropic, Neo-Hookean for rubber (Table 3) with strain energy potential [26,27]

$$U = C_{10}(\bar{I}_1 - 3) + \frac{1}{D_1}\left(J^{el} - 1\right)^2, \tag{4.2}$$

where: U – the strain energy potential, C_{10} – material constant related to the shear behavior, D_1 – material constant related to the compressibility, $\bar{I}_1$ – the first deviatoric strain invariant, J^{el} – the elastic volume ratio.

- Hyperfoam for mineral wool (Fig. 5) with strain energy potential [28]

$$U = \sum_{i=1}^{N} \frac{2\mu_i}{\alpha_i^2}\left[\widehat{\lambda_1}^{\alpha_i} + \widehat{\lambda_2}^{\alpha_i} + \widehat{\lambda_3}^{\alpha_i} - 3 + \frac{1}{\beta_i}\left(\left(J^{el}\right)^{-\alpha_i\beta_i} - 1\right)\right], \tag{4.3}$$

where: U – the strain energy potential, N – material parameter, α_i – temperature-dependent material parameters, μ_i – material parameter related to the initial shear modulus, β_i – material parameter determines the degree of compressibility, λ_i – principal stretches, J^{th} – the thermal volume ratio, $\widehat{\lambda_i} = \left(J^{th}\right)^{-1/3}\lambda_i$, J^{el} – the elastic volume ratio.

The parameters of mineral wool were introduced using Uniaxial Test Data, using the stress-strain relationship (Fig. 5) for the compression of the mineral wool sample [29]. Wet weight of 300 kg/m^3 was assumed.

- Cohesive Behavior, uncoupled traction for adhesive layer (Table 4) [30,31] with the stress-strain relation

$$\boldsymbol{t} = \begin{Bmatrix} t_n \\ t_s \\ t_t \end{Bmatrix} = \begin{bmatrix} K_{nn} & 0 & 0 \\ 0 & K_{ss} & 0 \\ 0 & 0 & K_{tt} \end{bmatrix} \begin{Bmatrix} \varepsilon_n \\ \varepsilon_s \\ \varepsilon_t \end{Bmatrix} = \boldsymbol{K\varepsilon}. \tag{4.4}$$

where: K_{nn} – the stiffness in the normal direction, K_{ss}, K_{tt} – the stiffness in the two shear directions, t_n – the normal traction, t_s, t_t – the shear tractions, $\varepsilon_n, \varepsilon_s, \varepsilon_t$ – the strain in normal and two shear directions, respectively.

The interface layer between the aluminum facing and the wool core was modeled using Interaction – Cohesive Behavior (Table 4). The uncoupled elasticity law for cohesive material with the criterion of maximum stress was used [30,31]:

$$\max\left\{\frac{\langle t_n \rangle}{t_n^0}; \frac{t_s}{t_s^0}; \frac{t_t}{t_t^0}\right\} = 1. \tag{4.5}$$

where: t_n, t_s, t_t – the normal and two shear tractions, respectively, t_n^0, t_s^0, t_t^0 – the peak value of normal and two shear tractions, respectively, $\langle\ \rangle$ – Macaulay brackets, means that the pure compressive does not initiate damage.

Table 2. Properties of elastic materials used in numerical analysis

	Young's modulus E [Pa]	Poisson's ratio ν [–]	Density γ [kg/m^3]
Aluminum	$0{,}7 \cdot 10^{11}$	0,33	2800
Steel	$2{,}1 \cdot 10^{11}$	0,30	7860
Concrete	$0{,}3 \cdot 10^{11}$	0,20	2500

Table 3. Material parameters for rubber

Density	γ [kg/m^3]	1100
Material dependent parameters	C_{10} [Pa]	$3{,}3345 \cdot 10^6$
	D_1 [1/Pa]	$3 \cdot 10^{-10}$

Table 4. Material parameters for adhesive [32]

Stiffness in the normal direction	K_{nn} [Pa]	$8{,}61 \cdot 10^6$
Stiffness in the shear direction	K_{ss} [Pa]	$4{,}22 \cdot 10^6$
	K_{tt} [Pa]	$4{,}22 \cdot 10^6$
Normal traction	t_n^0 [Pa]	$1{,}23 \cdot 10^5$
Shear traction	t_s^0 [Pa]	$1{,}12 \cdot 10^5$
	t_t^0 [Pa]	$1{,}12 \cdot 10^5$

Furthermore, in the model, General Contact functionality was applied. Additionally, the exceptions for individual panels and the ground beam were included friction coefficient 0,30 for a panel – panel contact, 0,35 for a panel – ground beam contact and 0,75 for a ground beam – pile contact. Due to the fact that the corrosion occurred above all in the lower part of the acoustic screen, only the lowest panel was modeled in details – the profiled shape, the perforation of the sheet and the connection between the panels were taken into account (Fig. 6). Other panels were modeled as a rectangular without the above details. Moreover, in the analysis, the whole column cross-section is considered due to the assumption that the panels on the other side of the column lost their load-bearing capacity and thus the possibility of transferring the load to the column.

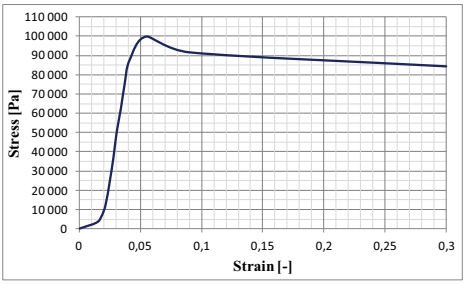

Fig. 5. Stress-strain relationship for compression of the mineral wool sample [29]

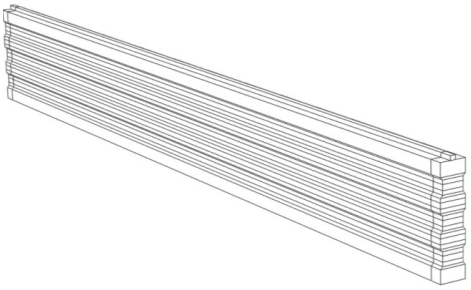

Fig. 6. The model of the lowest panel

The numerical model of the acoustic screen is presented in Fig. 7. For wool core, ground beam and foundation piles C3D8R finite elements (eight-node linear brick elements with reduced integration) were used. In addition, hourglass control was used for the detailed wool core. The facings and columns were modeled using S4R four-node shell elements [33].

Finally, a set of different constraints were added to make the structure as a whole. The TIE connection was used between the following elements: column – gasket, gasket – C-section, C-section – cladding, column base – foundation pile.

Next, for the connection of the core and the cladding two models are created – first, they were connected by TIE due to the fact that the facings should not be torn from the core; in the second they were connected by the Cohesive Surface to model a real occurrence of glue between these elements. This modeling method has been applied only for the lowest panel (yellow surface in Fig. 8) – for the remaining panels, a TIE connection was used only (blue surface in Fig. 8).

The acoustic screen was fixed in piles. This assumption results from the unavailability of geotechnical documentation of the ground subsoil occurring in the area of the considered acoustic screens. Therefore, the lateral resistance of the soil to the side of the pile or the correctness of pile foundation design is not considered and the attention is focused on the correctness of the applied construction solutions of the other elements of the acoustic screen. Moreover, the possibility of displacement in the X direction was blocked on steel columns. The boundary conditions are presented in Fig. 9.

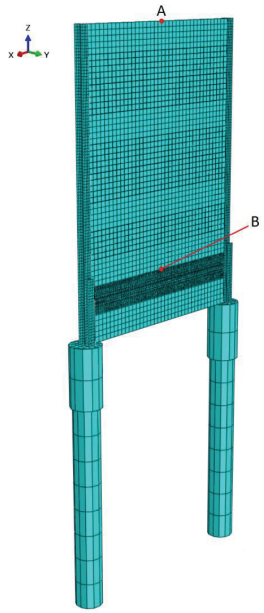

Fig. 7. Model with finite element mesh

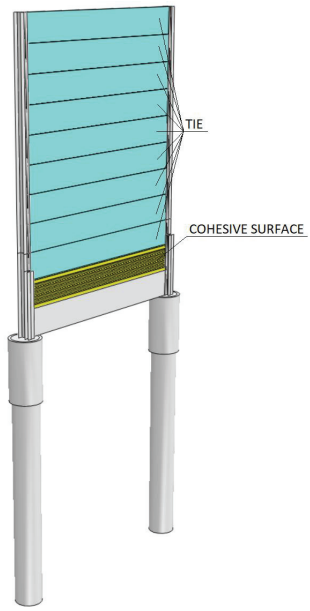

Fig. 8. TIE and Cohesive Surface

Fig. 9. Boundary conditions

5. THE NUMERICAL ANALYSIS

The analysis was started by replacing the perforated sheet model with a simplified model (see Fig. 10). The accurate cladding has square holes with dimensions of 8 x 8 mm. This involves the use of a dense mesh of finite elements (this model consisted of 601 363 finite elements), which means long computation time. Therefore, the equivalent model was created. Simplification in the model involves the use of full sheet metal, but with a smaller thickness in zones where holes are. Thickness in these places was selected so that the stiffness of both models was equal. This condition is fulfilled for a thickness of 0,45 mm. The equivalent model consisted of 71 563 finite elements.

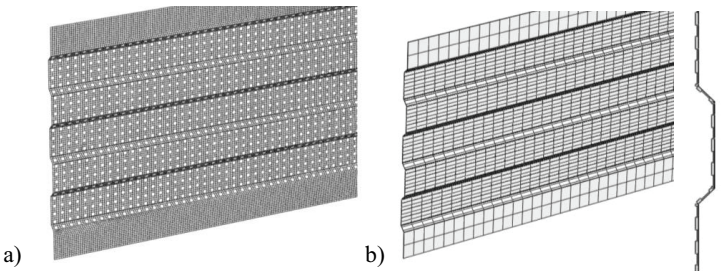

a) b)

Fig. 10. A numerical model of the perforated sheet a) detailed, b) equivalent

Static analysis for wind load and dynamic analysis for the load caused by car traffic was accomplished. Due to the non-linearity of the material models, a non-linear analysis was required.

5.1. STATIC ANALYSIS

The computations were performed using the Newton–Raphson method [34]. Wind load was determined according to the Eurocode [35] – a pressure was calculated as for a free-standing wall for a group of screens with a length of 740 m and a height of 5,5 m, 1-st load zones and III terrain category. The computational value of this load is 1656 Pa and it was applied to the entire surface of the screen in direction 1 shown in Fig.11a. Calculations were carried out for a model with a TIE and a Cohesive Surface connection for the bottom panel.

Including contact in the model caused an unstable system response and convergence problems [34], therefore contact stabilization was added. Damping has been added by the use of automatic stabilization for the whole model at energy dissipation intensity equal to the default value of 0,0002. The obtained results are discussed in Section 6.

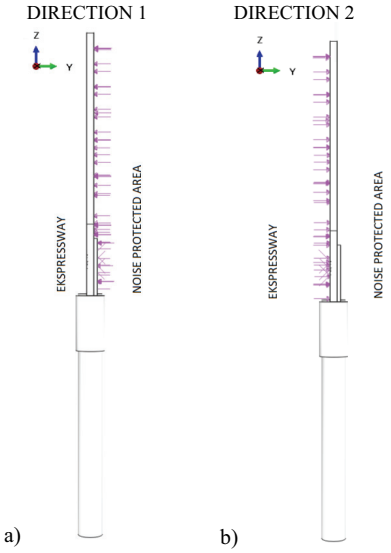

Fig. 11. Load direction

5.2. DYNAMIC ANALYSIS

Dynamic analysis began with solving the eigenvalue problem [36] and determining the frequency and the form of natural vibrations. Fig. 12 shows the first four eigenvectors.

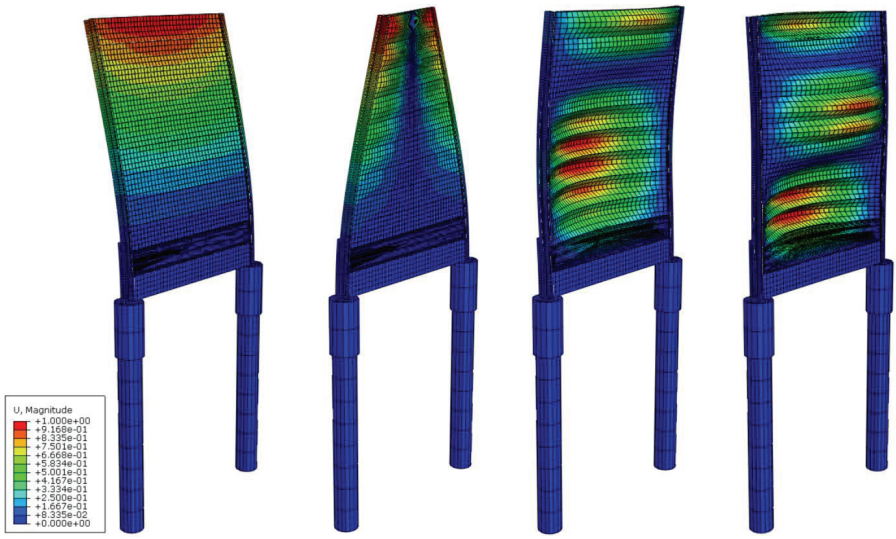

$f_1 = 4{,}1742$ Hz $f_2 = 7{,}7614$ Hz $f_3 = 12{,}047$ Hz $f_4 = 14{,}249$ Hz

Fig. 12. Frequency and the form of natural vibrations for the first four eigenvectors

In order to check the impact of the load derived from passing vehicles on the behavior of the acoustic screens, dynamic analysis was used. The acoustic screens are located on the expressway – road traffic takes place in the open air at a distance of 3,75 m at a maximum speed of 120 km/h, therefore according to [9] the computational value of the load is 1200 Pa.

The load was applied to the entire surface of the screen in direction 2 shown in Fig. 11b conforming to the amplitude presented in Fig. 13. Within 0,12 s, the load reaches its maximum value and reaches zero within the next 0,12 s. This amplitude reflects the passage of 10 cars, one behind the other at a distance of 60 m between them, so this load was repeated at intervals of 1,74 s in ten cycles.

In order to understand the role of the nonlinearity which is caused by material definition, cohesive property and contact two solution strategies were considered. The first includes linear Modal Dynamic analysis [37] without damping. The aim was to determine the moment of time t, for which the maximum swing from the equilibrium position will occur. Fig. 14 and Fig. 15 shows the displacement – time graph for the highest point (point A in Fig.7) and for the point on the lowest panel (point B in Fig.7), respectively.

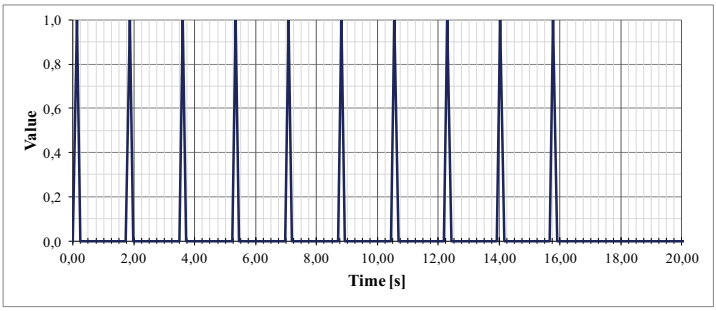

Fig. 13. The amplitude of air pressure load derived from the group of 10 cars

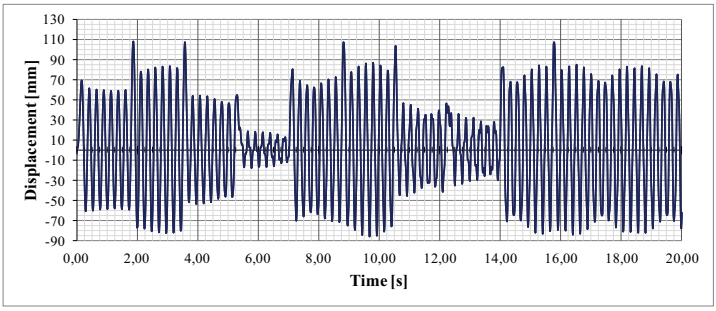

Fig. 14. Relationship horizontal displacement – time for the load derived from a group of vehicles for point A (cf. Fig.7)

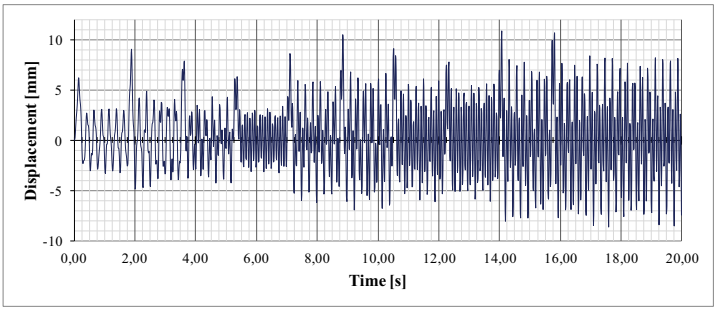

Fig. 15. Relationship horizontal displacement – time for the load derived from a group of vehicles for point B (cf. Fig.7)

Analyzing the displacement – time relation it was noticed that in the initial period (time $t = 0 \div 5{,}25$ s), the vibrations of the acoustic screen correspond with the first eigenvector (vibration period is 0,24 s, frequency 4,17 Hz), which is related with the deflection of the entire screen (see Fig. 12_1). In a further period of time, the passage of subsequent vehicles causes the vibration period to change to 0,07 s ($f = 14{,}28$ Hz), which causes excitation of the fourth eigenvector (see Fig. 12_4), which is associated with increased activity of the lower part of the acoustic screen.

Because the Modal Dynamic is linear, as mentioned, and does not take into account non-linearities, which may cause the displacement results to be overstated, so a non-linear analysis was performed also. For Modal Dynamic analysis, the maximum deflection was noted in 1,86 s. This information was used to limit the duration of the Dynamic Implicit analysis [38]. Fig. 16 presents a comparison of the results for these analyses. The obtained results are discussed in Section 6.

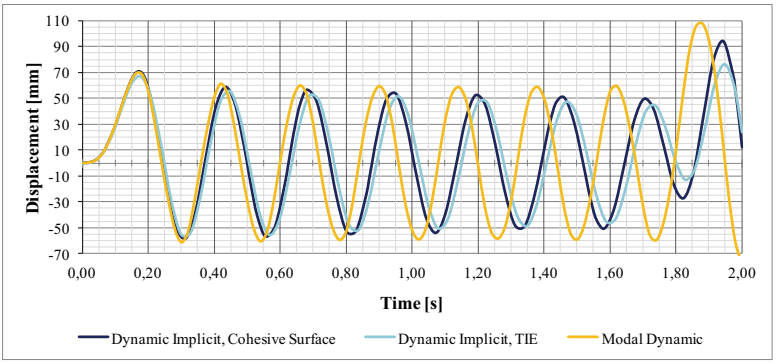

Fig. 16. Comparison of Dynamic Implicit and Modal Dynamic analysis

6. DISCUSSION OF RESULTS

The results of the analyzes are summarized in Table 5, while Table 6 shows the column deflection, that is 56,8 mm for static analysis, 68,0 mm and 83,6 mm for dynamic analysis, respectively for TIE and Cohesive Surface connection. The limit value determined by the standard [9] is 36,67 mm. It can be seen that in each analyzed case the permissible column deflection was exceeded (by 55% for the static analysis, by 85% and 128% for dynamic analysis, respectively for TIE and Cohesive Surface connection). This means that the column was designed incorrectly which caused severe deterioration.

Table 5. Results of analyzes

Type of analysis	A connection method of the cladding with the core	Deflection [mm]		
		Column	Top panel	Lower panel
Static, General	TIE	56,83*	14,00	11,18
	Cohesive Surface	56,78*	13,99	13,43
Dynamic Implicit	TIE	68,03*	17,68	7,45
	Cohesive Surface	83,61*	21,70	12,43
Limit value		36,67	50,00	50,00
* means that the limit value has been exceeded				

Table 6. Column deflection

Static, General	Dynamic, Implicit	
	TIE	Cohesive Surface
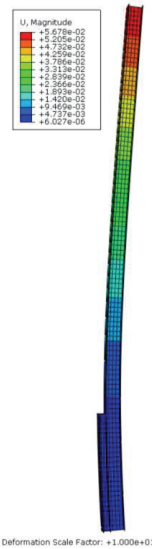	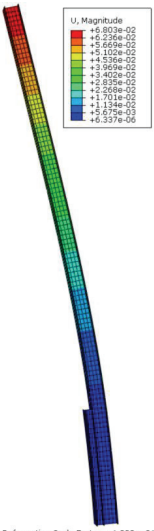	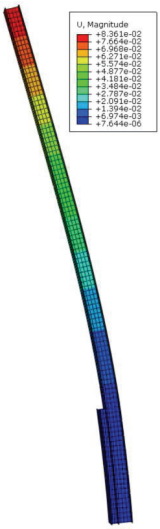
Deflection: 56,8 mm	Deflection: 68,0 mm	Deflection: 83,6 mm

Furthermore, due to the fact that the Eurocode [9] specifies that separation between individual panels should be avoided, the size of the contact opening between individual panels was checked in depending on the type of analysis and the type of connection between the core and the facing (see Table 7). The size of the contact opening between the panels is to be considered as unacceptable if it allows grains of sand or salt to enter. The most commonly used de-icing material is salt, which consists of 0.5 mm to 1 mm fraction [39]. Also, sand is used as a slippage prevention measure. According to [40] sand is an aggregate with a grain size of 0.063 mm to 2 mm. The highest value of contact opening occurs between panel no. 1 (P1) and panel no. 2 (P2) for the Cohesive Surface connection. It is approximately 0,752 mm for static analysis and 1,279 mm for dynamic analysis. The second largest value occurred between panel no. 1 (P1) and ground beam (GB) and it is a 0,316 mm for static analysis and 0,612 mm for dynamic analysis. These values are greater than the minimum size of sand and road salt grain and therefore sufficient to initiate crevice corrosion in highly aggressive environments, so these places can be regarded as critical.

Critical sites obtained as a result of numerical analysis are consistent with places with the highest corrosion occurrence in the discussed acoustic screen (Fig. 17). This convergence allows to conclude that the assumption regarding the detailed modeling of only the lower part of the acoustic

screen was correct. However, for a TIE connection, the separation between the panels is less than for Cohesive Surface. This means, that the stiffness of the connection between the cladding and the core must be taken into account during design.

Table 7. Contact opening

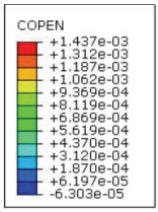

	Static, General		Dynamic, Implicit	
	TIE	Cohsive Surface	TIE	Cohsive Surface
P10	[mm]	[mm]	[mm]	[mm]
P9	0,176	0,176	0,187	0,229
P8	0,122	0,122	0,116	0,144
P7	0,094	0,090	0,078	0,083
P6	0,048	0,000	0,048	0,049
P5	0,000	0,000	0,060	0,068
P4	0,006	0,004	0,099	0,117
P3	0,045	0,042	0,177	0,215
P2	0,098	0,098	0,265	0,298
P1	0,424	**0,752**	0,102	**1,279**
GB	0,058	**0,316**	0,166	**0,612**

P1-P10 – panel with the appropriate number, GB – ground beam

Fig. 17. Corroded acoustic screen

7. CONCLUSIONS

Acoustic screens are applied to reduce noise caused by road traffic, therefore they are located near the road lane. Consequently, they are found in an environment of very high corrosivity. This article presents the numerical analysis of the acoustic screen located on the expressway, which was heavily corroded. The analysis was carried out to explain the causes of corrosion.

The construction of the acoustic screen and the basic requirements for the design of acoustic screens were presented. Eurocode [9] gives primarily limits for horizontal displacements of structural and acoustic elements and only indicates that road noise barrier should be designed so as to prevent corrosion. In the analyzed acoustic screen corrosion occurred primarily in its lower part. For this reason, special attention has been paid to the precise modeling of the lowest acoustic panel.

Static analysis for wind and dynamic analysis for load derives from vehicles were carried out. The obtained results were compared with the limit value, proving that the maximum deflection of columns was exceeded. The occurrence of separation between the panels where water and dirt can be accumulated was examined also. It was noticed that the largest contact opening occurred between panel P1 and panel P2. These sites are consistent with the place where the greatest corrosion damage was observed. Additionally, during analysis, it was noticed that the glue should be considered as a connection between the cladding and the core – unsticking of the cladding affects the increase of the contact opening value.

Moreover, the dynamic nature of the load derived from vehicles should be taken into account. For the dynamic analysis larger values were obtained, both the deflections of individual elements and the gap between the panels. Analyzing the structural response to the load derived from vehicles, it was noticed that the form of natural vibration related to the activity of the lower part of the acoustic screen was excited. This fact has a decisive effect on the occurrence of corrosion in this place.

In conclusion, the corrosion of the presented acoustic screen resulted from incorrect design – maximum deflection of columns was exceeded, which caused crevices between the panels. It has also been shown that the contact opening is influenced by the stiffness of the connection between the cladding and the core. Additionally, the dynamic nature of the load should be taken into account, due to the fact that the results obtained in the dynamic analysis are higher than in the static analysis. Furthermore, excitation of vibration associated with the movement of the lower panels, together with the pollution of the space between the panels with fine grains, resulted in greater exposure to abrasion of the protective aluminum coating in this part of the acoustic screen. What is more, the obtained outcomes could be even twice more unfavorable from the point of view of

Eurocode restrictions if the continuity of the whole screen would be assumed, as well as limited resistance of the soil and assembly errors of the structure would be taken into account.

REFERENCES

1. W. Drozd, "Acoustic baffles as a method of reduction of noise emission in the road infrastructure", Przegląd Budowlany, vol. R. 84, nr 12, 2013 (in Polish).
2. B. Kotzen and C. English, "Environmental Noise Barriers: A Guide To Their Acoustic and Visual Design", Second Edition. London: E & FN SPON, 1999.
3. M. Garai and P. Guidorzi, "European methodology for testing the airborne sound insulation characteristics of noise barriers in situ: experimental verification and comparison with laboratory data", The Journal of the Acoustical Society of America, vol. 108, no. 3, p. 1054, 2000.
4. T. Ishizuka and K. Fujiwara, "Performance of noise barriers with various edge shapes and acoustical conditions", Applied Acoustics, vol. 65, no. 2, pp. 125–141, 2004.
5. J. Y. Hong and J. Y. Jeon, "The effects of audio–visual factors on perceptions of environmental noise barrier performance", Landscape and Urban Planning, vol. 125, pp. 28–37, May 2014.
6. J. L. R. Joynt and J. Kang, "The influence of preconceptions on perceived sound reduction by environmental noise barriers", Science of The Total Environment, vol. 408, no. 20, pp. 4368–4375, Sep. 2010.
7. A. Behar and D. N. May, "Durability of sound absorbing materials for highway noise barriers", Journal of Sound and Vibration, vol. 71, no. 1, pp. 33–54, 1980.
8. "EN 14389-2:2004 - Road traffic noise reducing devices - Procedures for assessing long term performance - Part 2: Non-acoustical characteristics".
9. "EN 1794-1:2003 - Road traffic noise reducing devices - Non acoustic performance Part 1: Mechanical performance and stability requirements".
10. "EN 1794-2:2003 - Road traffic noise reducing devices - Non acoustic performance Part 2: General safety and environmental requirements".
11. X. Xiong, A. Li, X. Liang, and J. Zhang, "Field study on high-speed train induced fluctuating pressure on a bridge noise barrier", Journal of Wind Engineering and Industrial Aerodynamics, vol. 177, pp. 157–166, 2018.
12. M. Lü, Q. Li, Z. Ning, and Z. Ji, "Study on the aerodynamic load characteristic of noise reduction barrier on high-speed railway", Journal of Wind Engineering and Industrial Aerodynamics, vol. 176, pp. 254–262, y 2018.
13. M. Tokunaga, M. Sogabe, T. Santo, and K. Ono, "Dynamic response evaluation of tall noise barrier on high speed railway structures", Journal of Sound and Vibration, vol. 366, pp. 293–308, Mar. 2016.
14. "EN ISO 12944-2:2017 - Paints and varnishes - Corrosion protection of steel structures by protective paint system - Part 2: Classification of environments".
15 "EN 60721-3-4:1995 - Classification of Environmental Conditions - Part 3: Classification of groups of environmental parameters and their severities Section 4: Stationary use at non-weatherprotected locations".
16. J. R. Davis, "Corrosion of Aluminum and Aluminum Alloys". ASM International, 1998.
17. J. Xiao and S. Chaudhuri, "Predictive modeling of localized corrosion: An application to aluminum alloys", Electrochimica Acta, vol. 56, no. 16, pp. 5630–5641, Jun. 2011.
18. F. Mansfeld and J. V. Kenkel, "Galvanic corrosion of Al alloys—III. The effect of area ratio", Corrosion Science, vol. 15, no. 4, pp. 239–250, Jan. 1975.
19. Z. Szklarska-Smialowska, "Pitting corrosion of aluminum", Corrosion Science, vol. 41, no. 9, pp. 1743–1767, Aug. 1999.
20. Y. Huang, C. Wei, L. Chen, and P. Li, "Quantitative correlation between geometric parameters and stress concentration of corrosion pits", Engineering Failure Analysis, vol. 44, pp. 168–178, Sep. 2014.
21. M. Cerit, K. Genel, and S. Eksi, "Numerical investigation on stress concentration of corrosion pit", Engineering Failure Analysis, vol. 16, no. 7, pp. 2467–2472, Oct. 2009.
22. G. F. Kennell, R. W. Evitts, and K. L. Heppner, "A critical crevice solution and IR drop crevice corrosion model", Corrosion Science, vol. 50, no. 6, pp. 1716–1725, Jun. 2008.
23. W. Sun, L. Wang, T. Wu, and G. Liu, "An arbitrary Lagrangian–Eulerian model for modelling the time-dependent evolution of crevice corrosion", Corrosion Science, vol. 78, pp. 233–243, Jan. 2014.
24. M. J. Schofield, "Corrosion", in Plant Engineer's Reference Book, Elsevier, 2002, pp. 33-1-33–25.
25. R. de Borst, M. A. Crisfield, J. J. C. Remmers, and C. V. Verhoosel, "Nonlinear Finite Element Analysis of Solids and Structures", 2 edition. Hoboken, NJ: Wiley, 2012.
26. A. Ali, M. H. Fouladi, and B. Sahari, "A review of constitutive models for rubber-like materials", American Journal of Engineering and Applied Sciences, vol. 3, pp. 232–239, 2010.

27. M. C. Boyce and E. M. Arruda, “Constitutive Models of Rubber Elasticity: A Review”, Rubber Chemistry and Technology, vol. 73, no. 3, pp. 504–523, Jul. 2000.
28. B. Storåkers, “On material representation and constitutive branching in finite compressible elasticity”, Journal of the Mechanics and Physics of Solids, vol. 34, no. 2, pp. 125–145, Jan. 1986.
29. A. Buska and R. Mačiulaitis, “The compressive strength properties of mineral wool slabs: Influence of structure anisotropy and methodical factors”, Journal of Civil Engineering and Management, vol. 13, no. 2, pp. 97–106, Jan. 2007.
30. M. L. Benzeggagh and M. Kenane, “Measurement of mixed-mode delamination fracture toughness of unidirectional glass/epoxy composites with mixed-mode bending apparatus”, Composites Science and Technology, vol. 56, pp. 439–449, 1996.
31. P. P. Camanho and C. G. Davila, “Mixed-Mode Decohesion Finite Elements for the Simulation of Delamination in Composite Materials”, NASA/TM-2002–211737, pp. 1–37, 2012.
32. J. Pozorska and Z. Pozorski, “The numerical model of sandwich panels used for specifying wrinkling stress”, Journal of Applied Mathematics and Computational Mechanics, vol. 13, no. 3, 2014.
33. “Abaqus Analysis User’s Manual (6.12) ”.
34. P. G. Bergan, G. Horrigmoe, B. Bråkeland, and T. H. Søreide, “Solution techniques for non−linear finite element problems”, International Journal for Numerical Methods in Engineering, vol. 12, no. 11, pp. 1677–1696, 1978.
35. “EN 1991-1-4:2005 - Eurocode 1: Actions on structures Part 1-4: General actions - Wind actions”.
36. R. G. Grimes, J. G. Lewis, and H. D. Simon, “A Shifted Block Lanczos Algorithm for Solving Sparse Symmetric Generalized Eigenproblems”, SIAM Journal on Matrix Analysis and Applications, vol. 15, no. 1, pp. 228–272, Jan. 1994.
37. J. Shaw and S. Jayasuriya, “Modal sensitivities for repeated eigenvalues and eigenvalue derivatives”, AIAA Journal, vol. 30, no. 3, pp. 850–852, Mar. 1992.
38. H. M. Hilber and T. J. R. Hughes, “Collocation, dissipation and [overshoot] for time integration schemes in structural dynamics”, Earthquake Engineering & Structural Dynamics, vol. 6, no. 1, pp. 99–117, Jan. 1978.
39. A. Ružinskas, M. Bulevičius, and H. Sivilevičius, “Laboratory investigation and efficiency of deicing materials used in road maintenance”, Transport, vol. 31, no. 2, pp. 147–155, Jun. 2016.
40. “EN ISO 14688-1:2006 - Geotechnical investigation and testing - Identification and classification of soil - Part 1: Identification and description” .

LIST OF FIGURES AND TABLES:

ANALIZA NUMERYCZNA EKRANU AKUSTYCZNEGO

Słowa kluczowe: ekran akustyczny, korozja, analiza numeryczna

STRESZCZENIE

Drogowe ekrany akustyczne stosuje się jako ochronę przed hałasem powodowanym przez ruch samochodowy. Ze względu na bezpośrednie sąsiedztwo pasa drogowego, znajdują się one w środowisku o bardzo wysokiej korozyjności. Problemem jest więc korozja metalowych okładzin paneli akustycznych, w związku z tym podczas projektowania konstrukcji tego typu należy mieć na uwadze ograniczenie możliwości powstania korozji.

W artykule zweryfikowano ekrany akustyczne zlokalizowane wzdłuż drogi ekspresowej, w których zaobserwowano silną korozję. Analizie podlegały ekrany akustyczne składające z paneli akustycznych w obudowie z aluminium. W pracy przedstawiono konstrukcję analizowanego ekranu oraz opracowano model numeryczny uwzględniający zaawansowany model panelu, w szczególności profilowany kształt, perforację blachy oraz rodzaj połączenia między okładziną i rdzeniem.

Następnie przeprowadzono analizę statyczną dla obciążenia wiatrem oraz analizę dynamiczną dla obciążenia wywołanego przez pojazdy oraz sprawdzono spełnienie wymagań przedstawionych w normie EN 1794-1 dla poszczególnych elementów składowych ekranu akustycznego. Uzyskane wyniki analiz porównano z wartościami dopuszczalnymi, wykazując nadmierne ugięcie słupów oraz w konsekwencji powstanie pomiędzy poszczególnymi panelami akustycznymi szczeliny wystarczającej do gromadzenia się czynników korozyjnych, w szczególności takich jak sól drogowa oraz piasek. Wykazano, że miejsca największego otwarcia styku pomiędzy panelami są zgodnie z miejscami występowania największej korozji analizowanych ekranów. Dodatkowo, przeprowadzone analizy dynamiczne ujawniły wzbudzenie postaci drgań mogącej się przyczynić do powstania korozji.

Podsumowując, przedstawione w pracy wyniki wskazały błędy konstrukcyjne i ich wpływ na powstanie silnej korozji oraz znaczenie analizy dynamicznej w projektowaniu ekranów akustycznych.

Received 26.09.2019, Revised 29.03.2020